A Stochastic Network Model of the Interaction Between Cardiac Rhythm and Artificial Pacemaker

Saul E. Greenhut, *Member, IEEE*, Janice M. Jenkins, *Senior Member, IEEE*, and Robert S. MacDonald

Abstract—**The electrical interaction between the heart and an artificial pacemaker is often complex. Because of the sophistication and diversity of dual-chamber device algorithms, even experienced cardiologists can have difficulty interpreting paced electrocardiograms (ECG's). In order to study heart–pacemaker interaction (HPI), a computer model of the cardiac conduction system has been developed which includes the effects of artificial pacemaker function and failure. The stochastic network model of cardiac conduction consists of five vertices, each representing a functional electrophysiologic element. Electrophysiologic multidimensional conditional probability functions determine the depolarization status of each vertex. The atrioventricular (AV) node is emulated using a mathematical model which includes the influence of past cycle lengths on AV nodal conduction time. Twenty-three classes of arrhythmias may be simulated and, for pacing simulation, one of 12 antibradycardia pacing modes may be chosen. Random effects of pacemaker malfunction including oversensing, undersensing, or failure-to-capture may be simulated through the use of probability distribution functions. This model should prove useful in the development of pacemaker algorithms, determining patient-specific pacemaker therapy, and predicting causes for apparent pacemaker malfunction. The model has been used in the development of an expert system to analyze paced ECG's for pacemaker function and malfunction.**

I. Introduction

DIAGNOSIS of dual-chamber paced ECG's for analysis of pacemaker function and malfunction is often a challenging task, even for the experienced clinician. This is largely due to the complexity of dual-chamber pacemaker algorithms and their variability among manufacturers. In addition, paced fusion, pseudofusion, and pseudo-pseudofusion[1] depolarizations may occur, further confounding the interpretation. The development of an automated paced ECG diagnosis algorithm, which incorporates information on specific pacemaker algorithms and patient-specific settings, would be a valuable aid in assessing pacemaker function and appropriate individual pacemaker specifications. In order to expedite the design of an automated paced ECG analysis system, a model of heart–pacemaker interaction has been developed which served as a *test-bed* for development of such a diagnosis algorithm [1], [2].

Models of the cardiac conduction system can assume varying degrees of complexity depending upon the purpose of the simulation and the information desired. A cardiac conduction model, designed for simulation of heart rhythm and pacemaker functionality, was developed in order to test algorithms for the diagnosis of paced ECG's. Models of the cardiac conduction system have been designed by others which represent the heart in much greater detail [3]–[5]. However, the purpose of this model was to represent the overall sequence of cardiac conduction, and was *not* intended to simulate myocardial repolarization, conduction through small portions of myocardium, or even to generate realistic ECG waveforms. The conduction model was designed in order to generate realistic conduction sequences of a wide variety of arrhythmias and to demonstrate the response to artificial pacemaker algorithms incorporated in this model. We desired a model which generates realistic sequences of P and R waves without including the complexity of underlying arrhythmic mechanisms. Malik [6] has demonstrated that a simple model is adequate for HPI simulation. In addition, the cardiac rhythm model through specification of easily measured electrophysiologic parameters could provide the basis for a rhythm or pacemaker function interpretation scheme. A phenomenological probabilistic model for cardiac rhythm based upon ECG waveform sequences has been developed and is presented here.

The network model presented has the unique aspect of being described by multidimensional conditional probability functions (CPF's) with electrophysiologic parameters. The CPF's provide a concise methodology for conduction system simulation in a manner which can be applied using generalized electrophysiologic parameters. At each vertex, a CPF exists which determines the depolarization status of that vertex, based upon previous vertex depolarizations. The use of CPF's allows a simple and consistent structure of the conduction system, and yet permits the simulation of many arrhythmias (Table III).

The response of the cardiac conduction system to any one of 12 antibradycardia pacing modes can be simulated in the model presented here. In addition, the model described is the first to simulate pacemaker malfunction by including

Manuscript received May 30, 1990. This work was supported in part by NSF Grant BCS-8909042 and by Telectronics Pacing Systems.

S. E. Greenhut is with the Applied Research Division, Telectronics Pacing Systems, Inc., Englewood, CO 80112.

J. M. Jenkins and R. S. MacDonald are with the Department of Electrical Engineering and Computer Science and the Bioengineering Program, University of Michigan, Ann Arbor, MI 48104.

IEEE Log Number 9210776.

[1] A paced fusion depolarization is the result of a spontaneous and paced myocardial depolarization occurring nearly simultaneously so that both conduct and are superimposed on one another. In pseudofusion, only the spontaneous depolarization conducts; however, the pacemaker stimulus is superimposed on the spontaneous depolarization. In pseudo-pseudofusion, the pacemaker stimulus from the alternate chamber is superimposed on the spontaneous depolarization.

appropriate cardiac, pacemaker, and noise distribution parameters. Arrhythmia parameters and programmable pacemaker parameters can be varied in order to determine optimal, patient-specific, arrhythmia-specific pacemaker settings. The cardiac response to artificial pacing can be observed and, given some basic electrophysiologic parameters, the conduction model may be used to simulate an actual patient. The pacemaker model has been designed to sense and pace the conduction system model as an artificial pacemaker senses and paces an arrhythmic heart.

II. The Model

A. Stochastic Network Representation of Heart–Pacemaker Interaction

A stochastic network has been chosen as well suited for representation of the cardiac conduction system. This is based on the premise that rhythm simulation lends itself to consideration of the cardiac conduction system as a set of discrete functional temporal entities. In addition, output events in the analysis of rhythm are typically limited to the consideration of atrial and ventricular, normal, abnormal, and paced depolarizations which occur with certain timing and probability depending upon the underlying arrhythmia.

The cardiac conduction system model consists of five primary vertices defined by the set

$$Q = \{q_0, q_1, q_2, q_3, q_4\} = \{S, A, N_P, N_D, V\} \quad (1)$$

where The AV node is partitioned to allow representation of

S = sinoatrial node,
A = atrial myocardium,
N_P = proximal section of atrioventricular node,
N_D = distal section of atrioventricular node, and
V = ventricular myocardium.

mid-AV nodal block, AV nodal rhythms, and simultaneous conduction in proximal and distal portions of the AV node during prolonged first degree AV block or during simultaneous anterograde/retrograde conduction.

The model is represented by a signal flow graph in Fig. 1. The *vertices* are represented by circles with connected states indicated by input and output *pathways*. Output *events* occur along transitions between certain vertices. The event set is defined as

$$Y = \{an, vn, aa, va, ap, up\}. \quad (2)$$

This output alphabet represents depolarization morphologies as classified on the ECG or intracardiac electrogram. The alphabet defines discrete output depolarizations as follow: an = atrial normal, vn = ventricular normal, aa = atrial abnormal, va = ventricular abnormal, ap= atrial paced, and vp = ventricular paced. Outputs are indicated along pathways in Fig. 1, and occur at the transition between vertices. No output is designated whenever a pathway is directed toward an SA or AV nodal vertex because output from these electrophysiologic tissues cannot be readily identified on the ECG. Normal and accessory pathways, both anterograde and retrograde, are represented. The network description differs from probabilistic

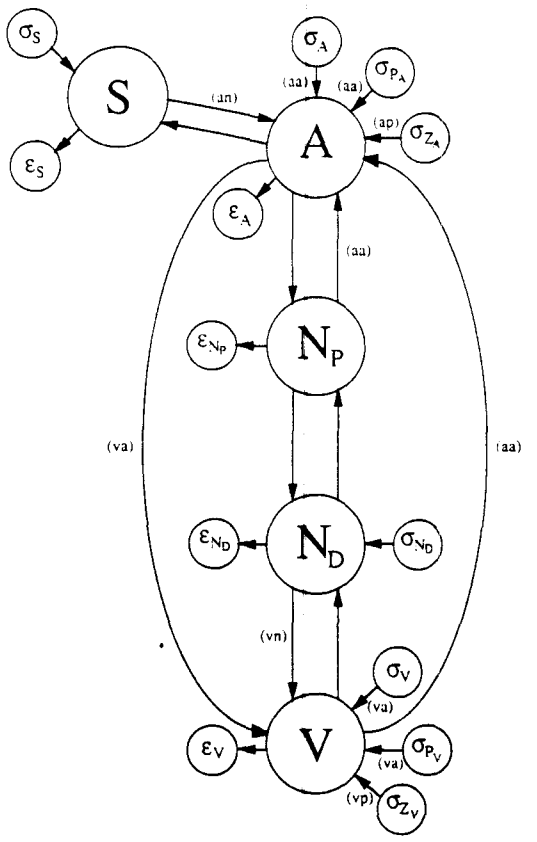

Fig. 1. Stochastic network model of cardiac rhythm. Vertices and pathways described in text. Output events are indicated along pathways within parentheses.

automata theory [7] in the following manner: more than one state may be active simultaneously; at any time, the sum of the exit probabilities at a given vertex is not equal to one; and current transitions depend upon the history of previous depolarizations. It also differs from timed stochastic Petri net theory [8], [9] for the two latter reasons and due to the absence of *tokens* controlling conduction. Probabilities of pathway conduction exist; however, these probabilities change dynamically and are not required to sum to one. Given the model structure, these deviations from standard theory are important to providing correct electrophysiologic function. More than one vertex, for instance, atrial and ventricular vertices, may depolarize simultaneously. The exit probabilities from a vertex do not usually equal one on a given cycle, allowing activation to remain at the same vertex over several cycles. Also, the history of previous depolarizations is important to determining when a vertex comes out of refractoriness and becomes autorhythmic.

A multidimensional conditional probability function (CPF) is defined at each primary vertex (S, A, N_P, N_D, V) which specifies, using electrophysiologic parameters, the timing and probability of depolarization at the vertex. Depolarization continues at a vertex for a time which depends upon the intervals and probabilities specified in the CPF of connecting vertices. The output vertex will depolarize at time t if its returned probability of conduction is greater than a pseudorandom number. Due to the nature of the CPF's, each vertex has a

probability of depolarizing; however, this probability changes dynamically with time and with the previous depolarization history of connected vertices. The returned probabilities at a given vertex are dependent upon the time since that vertex was last activated and upon the time since all connected vertices were last activated. Particular arrhythmias are specified by defining various electrophysiologic intervals and probabilities at each vertex. In this way, a wide variety of arrhythmias may be logically specified using an identical structure for each arrhythmia. Each of the CPF's is described in detail in the next section.

In addition to the five primary vertices defined above, vertices designated by σ and ϵ are included in the signal flow graph of Fig. 1. Each of the σ's represents possible depolarization initiation at a primary vertex. Initiation may cause normal, abnormal, or paced activity. The σ vertices are defined as follows: σ_S = SA node autorhythmic vertex, σ_A = atrial ectopic vertex, σ_{N_D} = AV node autorhythmic vertex, σ_V = ventricular ectopic vertex, σ_{P_A} = atrial parasystolic vertex, σ_{P_V} = ventricular parasystolic vertex, σ_{Z_V} = atrial paced vertex, and σ_{Z_V} = ventricular paced vertex. Note that σ_{N_P} does not exist since N_P serves only as a conduction vertex (i.e., spontaneous initiation of depolarization is not allowed at N_P). This is not a serious limitation for a model of cardiac rhythm since the distal section of the node N_D can initiate impulses. Therefore, simulation of AV nodal rhythms is possible. The AV node is divided into two elements to allow visualization of AV nodal block and rhythms, as well as to permit simultaneous anterograde and retrograde conduction within (different portions of) the node. The parasystolic vertices represent myocardium which, when activated, cause asynchronous abnormal depolarizations in a regular, repeating fashion. Timing algorithms control transitions from parasystolic and paced vertices.

Once activation has occurred at a primary vertex, the system will conduct given that the returned conditional probability of conduction is greater than the random number at some time during the permitted conduction interval. If conduction does not occur during specified anterograde or retrograde conduction intervals, electrophysiologic block occurs (unless it occurs in the anterograde direction at the ventricular vertex). Conduction endpoints are designated by ϵ's in the graph of Fig. 1. Since block may occur anywhere in the system, one ϵ vertex is connected to each cardiac element vertex.

The normal conduction sequence would be represented by the transition sequence

$$\sigma_S \rightarrow S \rightarrow A \rightarrow N_P \rightarrow N_D \rightarrow V \rightarrow \epsilon_V.$$

Activation initiates at the SA node, followed by normal atrial output (an), traversal through the AV node (no output), followed by a normal ventricular event (vn), and termination of conduction. There exists more than one rhythm diagnosis for a given transition sequence, as the time spent at a given vertex is an important factor in determining relationships between events. The timing within and between states is controlled by electrophysiologic CPF's discussed below.

B. Model Sequence and Timing Description: Conditional Probability Functions

In order to specify cardiac rhythms, a mechanism for regulating the timing of conduction between vertices has been developed. The probability of vertex depolarization at a particular time is determined by multiple probability functions conditioned on the time since the previous depolarization of each connecting vertex. The form of these conditional probabilities has been developed to correspond to realistic electrophysiologic characteristics of the cardiac conduction system. The CPF of each vertex returns a probability of conduction at each sample point (every 5 ms in the examples of Figs. 10–15). This probability is compared to a computer-generated uniformly distributed pseudorandom number between 0 and 1. If the probability of conduction at a vertex is greater than the random number, the vertex depolarizes; otherwise, it does not, and the time since the previous depolarization t_{vertex} is incremented. If more than one type of depolarization is plausible at a given time, the algorithm returns the type corresponding to the maximum probability of occurrence. The uniformly distributed pseudorandom number generation introduces pseudorandom beat-by-beat variability, while the vertex CPF's govern overall rhythm statistics. Parameters at each vertex, specified in detail in Table I, consist of the following general electrophysiologic variables:

- Vertex absolute refractory periods
- Probabilities of vertex escape depolarization
- Vertex escape intervals
- Probabilities of pathway conduction
- Pathway conduction intervals, and
- AV node vertex conduction parameters.

1) Sinoatrial (SA) Node Vertex: SA node timing is based upon the interval since the preceding SA node activation and the time since the preceding atrial depolarization. This is shown in Fig. 2(a) as a two-dimensional conditional probability function: $P(S|t_S, t_A)$.[2] For this vertex, a three-dimensional perspective of the CPF with plausible parameters is shown in Fig. 2(b) in order to better visualize the changing probability. Any time since the previous SA node depolarization t_S which is less than the SA node absolute refractory period t_R, the probability of SA depolarization equals 0. Premature SA depolarizations (as in sinus arrhythmia) may occur if $P_{E_{MAX}}$ is set greater than 0. P_E increases linearly from 0 to $P_{E_{MAX}}$ as t_S increases from t_R to t_{A_1}. P_A increases linearly from 0 to $P_{A_{MAX}}$ as T_S increases from t_{A_1} to t_{A_2} and then remains constant at $P_{A_{MAX}}$ after t_{A_2} as long as $t_A > t_{RC_2}$ or $t_A < t_{RC_1}$. On the t_A axis, time since the previous atrial depolarization, there is one atrial interval to consider. If while $t_{RC_1} < t_A < t_{RC_2}$, $t_R < t_S < t_{A_1}$, the probability of conduction from the atria to the SA node, P_{RC}, increases linearly from 0 to $P_{RC_{MAX}}$ as t_A approaches t_{RC_2}. This occurs in the case of SA node reset following either a premature atrial depolarization or atrial retrograde conduction. Within this interval, $P(S) = \max(P_{RC}, P_E)$. Finally, if $t_{RC_1} < t_A < t_{RC_2}$ and $t_S > t_{A_1}$, $P(S) = \max(P_{RC}, P_A)$.

[2] In the following discussion, t_{vertex} refers to the time elapsed since the previous depolarization at the given vertex.

TABLE I
CONDITIONAL PROBABILITY FUNCTION ELECTROPHYSIOLOGIC PARAMETERS

Parameter	Definition
P_A	The instantaneous probability of an escape depolarization initiating at a vertex which increases linearly from $0 \rightarrow P_{A_{MAX}}$.
$P_{A_{MAX}}$	The maximum probability of an escape depolarization. Rhythm specific parameter entered by the user.
P_C	The instantaneous probability of anterograde conduction along a normal pathway between two vertices which increases linearly from $0 \rightarrow P_{C_{MAX}}$. P_C, refers to anterograde accessory pathway conduction.
$P_{C_{MAX}}$	The maximum probability of anterograde conduction along a normal pathway between two vertices. Rhythm specific parameter entered by the user. $P_{C'_{MAX}}$ refers to anterograde accessory pathway conduction.
P_{RC}	The instantaneous probability of retrograde conduction between two vertices which increases linearly from $0 \rightarrow P_{RC_{MAX}}$. P_{RC}, refers to retrograde accessory pathway conduction.
$P_{RC_{MAX}}$	The maximum probability of retrograde conduction between two vertices. Rhythm specific parameter entered by the user. $P_{RC'_{MAX}}$ refers to retrograde accessory pathway conduction.
P_E	The instantaneous probability of an early, ectopic depolarization at a vertex which increases linearly from $0 \rightarrow P_{E_{MAX}}$.
$P_{E_{MAX}}$	The maximum probability of an early, ectopic depolarization at a vertex. Rhythm specific parameter entered by the user.
t_R	Absolute refractory period. At $t < t_R$, the element cannot depolarize ($P = 0$).
$t_{A_1} \rightarrow t_{A_2}$	Automatic interval. At $t_{A_1} < t < t_{A_2}$, P increases linearly from 0 to P_A. At $t \geq t_{A_2}$, $P = P_{A_{MAX}}$.
$t_{C_1} \rightarrow t_{C_2}$	Anterograde conduction interval. At $t_{C_1} < t < t_{C_2}$ after depolarization of the previous vertex, the current vertex may be activated with $P = P_C$. Primed parameters indicate anterograde accessory pathway conduction times.
$t_{RC_1} \rightarrow t_{RC_2}$	Retrograde conduction interval. At $t_{RC_1} < t < t_{RC_2}$ after depolarization of the previous vertex, the current vertex may be activated with $P = P_{RC}$. Primed parameters indicate retrograde accessory pathway conduction times.
$t_{CT_{LIM}}$	Conduction time limit for the AV node such that when $t > t_{CT_{LIM}}$, $P = 0$. The parameter is used only in the probability function for N_P (anterograde) and N_D (retrograde) vertices. When $t \leq t_{CT_{LIM}}$, $P = P_C$ or $P = P_{RC}$.

2) Atrial Vertex: Since the atrium may depolarize in either an anterograde or retrograde manner, the depolarization sequence of the atria is based upon the time since the SA node, atria, AV node, and ventricles last depolarized: $P(A|t_S, t_A, t_{N_P}, t_V)$. This four-dimensional probability is most easily described by three separate two-dimensional graphs. As with the SA vertex, whenever unequal probabilities intersect, the probability and resultant depolarization type with the largest value is selected for comparison with the generated random number. The resulting probability may be stated as

$$P(A|t_S, t_A, t_{N_P}, t_V)$$

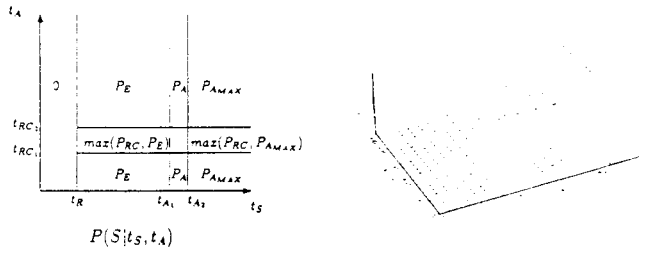

Fig. 2. (a) SA node vertex conditional probability function. (b) Three-dimensional perspective of an example SA node vertex CPF. Similar examples could be drawn for the remaining vertices. Because of the nonlinearity when $t_{RC_2} < t_A < t_{RC_1}$, the form of the CPF will change in this interval, depending upon the relationship between P_{RC} and P_E. The parameters in this example are: t_R = 300 ms, t_{A_1} = 850 ms, t_{A_2} = 900 ms, t_{RC_1} = 150 ms, T_{rc_2} = 300 ms, $P_{E_{MAX}}$ = 0.5, $P_{RC_{MAX}}$ = 0.75, and $P_{A_{MAX}}$ = 1.0.

$$= \max(P(A|t_S, t_A), P(A|t_{N_P}, t_A), P(A|t_V, t_A)). \quad (3)$$

This is shown in Fig. 3 (a)–(c) in which the x axis and values of P_E, P_A, and $P_{A_{MAX}}$ are the same throughout. Differences are seen in the y axes as probabilities of conduction between any vertex and the atria.

The x axes indicate time since previous atrial depolarization t_A. As for the SA node, $P(A) = 0$ at times less than t_R. Analogous to the SA node vertex, there exists a region where probability of premature atrial activation increases linearly ($t_R < t_A < t_{A_1}$), while at $t_A > t_{A_2}$, atrial automatic (escape) depolarizations occur with $P(A) = P_{A_{MAX}}$.

Each y axis represents the time since adjacent vertex depolarizations. The time since SA activation t_S [Fig. 3(a)] indicates anterograde conduction time from the SA node to the atria by the range $t_{C_1} < t_S < t_{C_2}$. At the intersection of this interval with $t_R < t_A < t_{A_1}$, $P(A) = \max(P_C, P_E)$, while at $t_A > t_{A_1}$, $P(A) = \max(P_C, P_A)$.

This conditional probability format of $P(A)$ is analogous for t_{N_P} and t_V, except that these reflect retrograde conduction times. Fig. 3(b) represents retrograde conduction through the AV node, with the conduction times (t_{RC_1} and t_{RC_2}) representing time between completion of proximal AV node depolarization and the beginning of atrial activation. Conduction from V to A through an accessory pathway is indicated in Fig. 3(c). Here, $P_{RC'}$ is the probability of retrograde conduction via an accessory pathway and $t_{RC'_1} < t_V < t_{RC'_2}$ is the VA accessory conduction time range.

3) AV Node Vertices: As described previously, the AV node is partitioned into a proximal and distal vertex. The proximal vertex serves as a conduction element only. Spontaneous (ectopic) depolarizations may occur only at the distal AV nodal element. Also, the conditional probability functions of the AV vertices include an additional variable: the AV nodal conduction time t_{CT}. The AV nodal conduction time, which depends on previous cycle lengths, is calculated prior to anterograde or retrograde penetration of the AV node. This is described in detail in a later section.

i) AV Node Proximal Vertex: Fig. 4 shows the probability functions for the AV proximal vertex. Fig. 4(a) and (b) represent anterograde conduction, while Fig. 4(c) depicts retrograde conduction. In Fig. 4(a), the calculated AV nodal

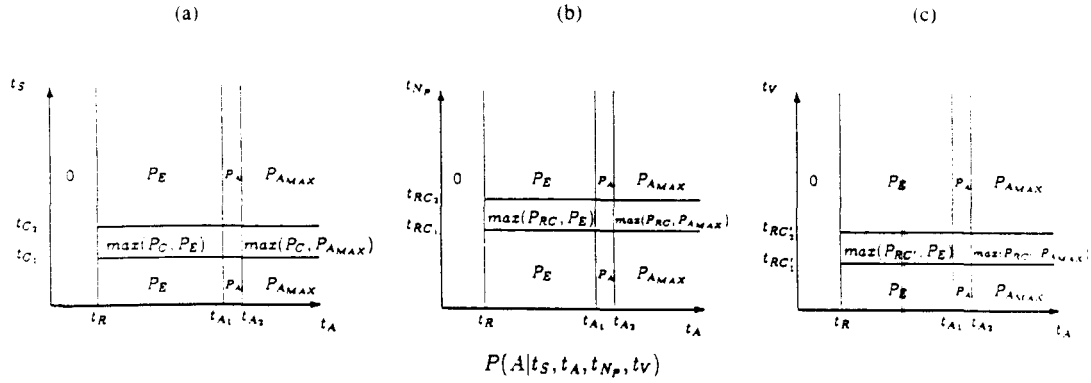

Fig. 3. Atrial vertex conditional probability function.

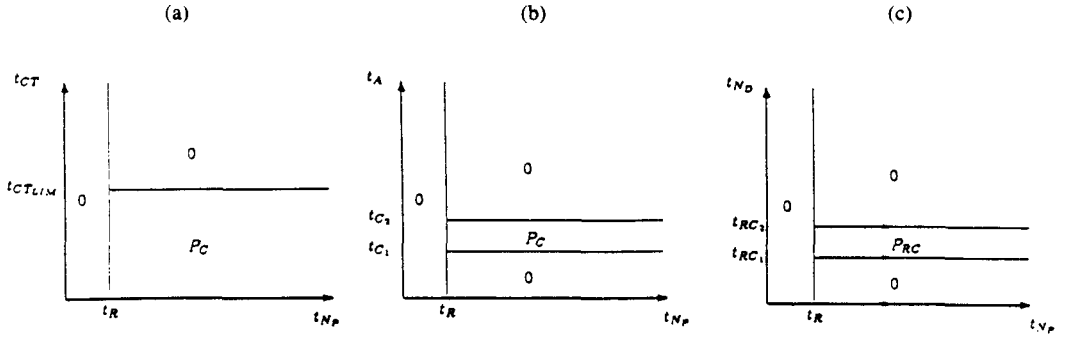

Fig. 4. Proximal AV node vertex conditional probability function.

conduction time t_{CT}, via the AV nodal model (described below), is represented on the y axis and the time elapsed from the previous AV proximal vertex depolarization t_{N_P} is given on the x axis. If t_{CT} is less than the AV nodal conduction time limit $t_{CT_{\text{LIM}}}$ and t_{N_P} is greater than the functional refractory period of the node, $P = P_C$. ($t_{CT_{\text{LIM}}}$ is the atrial extra stimulus A_2H_2 interval corresponding to the effective refractory period as determined on the patient's AV nodal conduction curve.) Note that there is no linear variability of P_C in Fig. 4(a), and that the condition in Fig. 4(b) *must also* be satisfied for conduction to occur. Also, there are no ectopic or automatic probabilities since activation may not be initiated at this vertex.

In Fig. 4(b), it is evident that a conduction time between atrial and AV nodal conduction may be specified. When $t_{C_1} < T_A < T_{C_2}$, anterograde depolarization of the proximal AV node occurs as long as the condition in Fig. 4(a) is satisfied. Therefore, depolarization of the proximal AV vertex anterogradely AD_{N_P} occurs with probability P_C if the following Boolean equation holds:

$$AD_{N_P} = (t_{N_P} > t_R) \wedge (t_{CT} < t_{CT_{\text{LIM}}}) \wedge (t_{C_1} < t_A < t_{C_2}). \tag{4}$$

Probability of retrograde conduction of the proximal AV vertex is graphically displayed in Fig. 4(c). Conduction will occur with probability P_{RC} once the distal AV vertex has retrogradely conducted for $t_{CT}/2$. The retrograde probability equals P_{RC} for one sample interval, then reverts to 0. Therefore, in Fig. 4(c), $t_{RC_1} = t_{CT}/2$ and $t_{RC_2} = (t_{CT}/2) + x_s$ ms, where x_s is the sampling interval.

ii) AV Node Distal Vertex: Anterograde conduction of the AV distal vertex is depicted by Fig. 5(a). In an analogous manner to retrograde conduction through the proximal vertex, if ($t_{C_1} = t_{CT}/2$) $< t_{N_P} <$ ($t_{C_2} = (t_{CT}/2) + x_s$ ms) and $t_{N_D} > t_R$, anterograde distal vertex conduction is possible. However, unlike the proximal vertex, early and escape depolarizations are also allowed. Their probabilities vary in a linear manner, and are indicated in Fig. 5(a) in a fashion analogous to the SA node and atrial vertices.

Fig. 5(b) and (c) show the probability function of retrograde conduction through the distal vertex. When combining the information from these graphs, it is evident that retrograde conduction from the ventricles to the distal AV vertex RC_{N_D} occurs with probability P_{RC} if the following Boolean equation holds:

$$\begin{aligned} RC_{N_D} = &(((t_R < t_{N_D} < t_{A_1}) \wedge (P_{RC} > P_E)) \\ &\vee ((t_{N_D} > t_{A_1}) \wedge (P_{RC} > P_A))) \\ &\wedge (t_{RC_1} < t_V < t_{RC_2}) \wedge (t_{CT} < t_{CT_{\text{LIM}}}) \\ &\wedge (t_{N_D} > t_R). \end{aligned} \tag{5}$$

Also indicated in Fig. 5(c) are probability time ranges for premature and escape depolarizations which conduct retrogradely. These probabilities increase linearly until a maximum is reached, and are represented in Fig. 5(c) in a manner analogous to sinus node and atrial vertices.

4) Ventricular Vertex: The ventricles depolarize based upon the time elapse since the previous atrial, distal AV nodal, or ventricular depolarization: $P(V|t_A, t_{N_D}, t_V)$. The explanation of the ventricular conditional probability function is

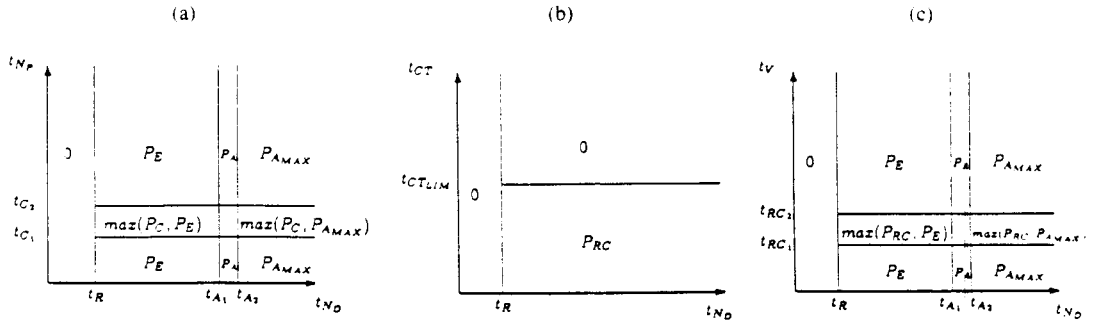

Fig. 5. Distal AV node vertex conditional probability function.

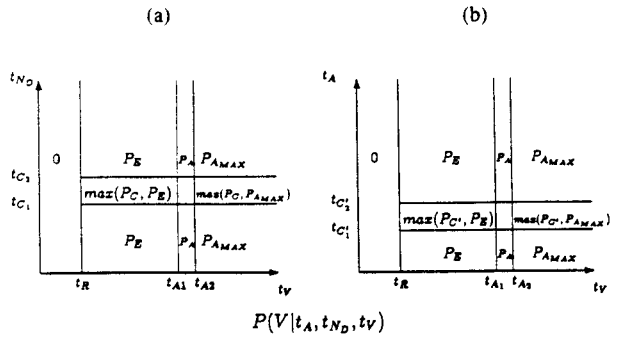

Fig. 6. Ventricular vertex conditional probability function.

consistent with those discussed previously for the SA and atrial vertices. Graphs describing its three-dimensional CPF are shown in Fig. 6. Fig. 6(a) represents anterograde conduction through the AV node, while Fig. 6(b) represents anterograde conduction through an accessory pathway. Premature and escape depolarizations are represented identically on both graphs.

5) Parasystolic Vertices: The timing of parasystolic atrial and parasystolic ventricular depolarizations, represented by σ_{P_A} and σ_{P_V}, may be considered simple one-dimensional probability functions. Each represents myocardium which depolarizes in a systematic fashion; therefore, the instantaneous probability of each vertex is dependent only upon the time since it last depolarized. Descriptions are identical, except that each occurs in a different chamber of the heart. There is no refractory period specified for these elements since they are defined as being unaffected by external sources. Parasystolic activation is represented on the ladder diagram or simulated ECG output as an ectopic depolarization.

An additional parameter, designated the *automatic depolarization phase shift*, is specified for parasystolic modeling of atrial and ventricular n-geminy. A parasystolic vertex is given an asynchronous rate and an offset from the chamber rate by this phase shift. Therefore, regular n-geminy is possible with specified coupling intervals between normal and parasystolic depolarizations.

C. Method of Vertex Timing Specification

In order to simulate a rhythm, parameters are entered into a rhythm-specific text data file incorporated into the conduction model algorithm. In order to generate different rhythms, the probability function parameters are set appropriately for each vertex. These input parameters are chosen based upon known electrophysiologic refractory periods, conduction intervals, and depolarization probabilities.

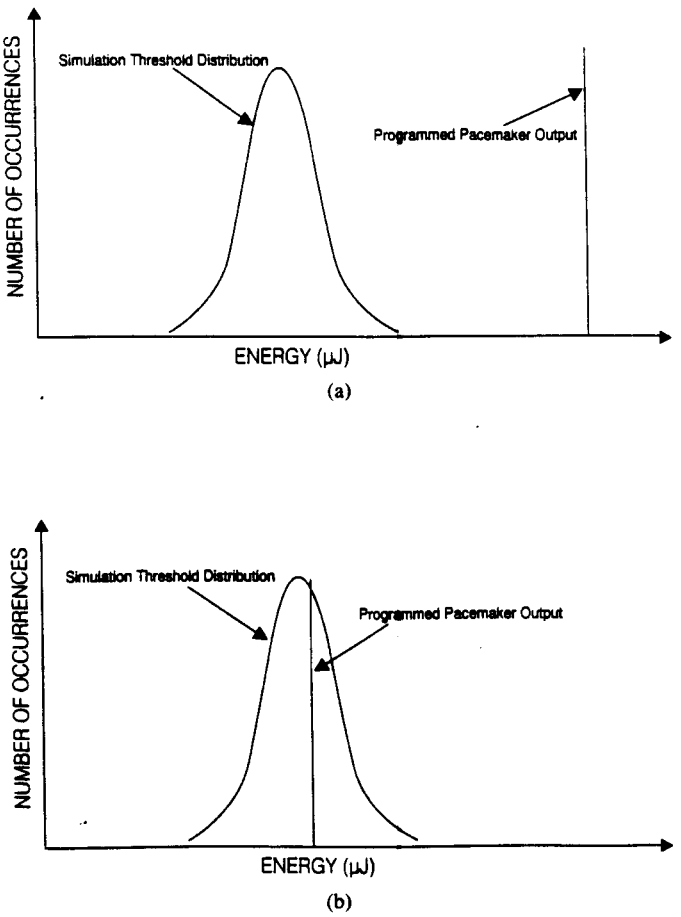

Fig. 7. Cardiac stimulation threshold—programmed pacemaker output relationship. Stimulation threshold is represented by a Gaussian distribution. (a) Pacemaker output (a function of pulse amplitude and width) is greater than the stimulation threshold with near 100% certainty. (b) Pacemaker output is well within the stimulation threshold distribution which would lead to failure-to-capture after approximately 40% of all pacemaker stimuli delivered.

D. Model of Atrioventricular (AV) Node Conduction

The AV node is the most complex functional electrophysiologic entity of the heart. Current AV conduction time is dependent upon preceding cycle lengths in an exponentially

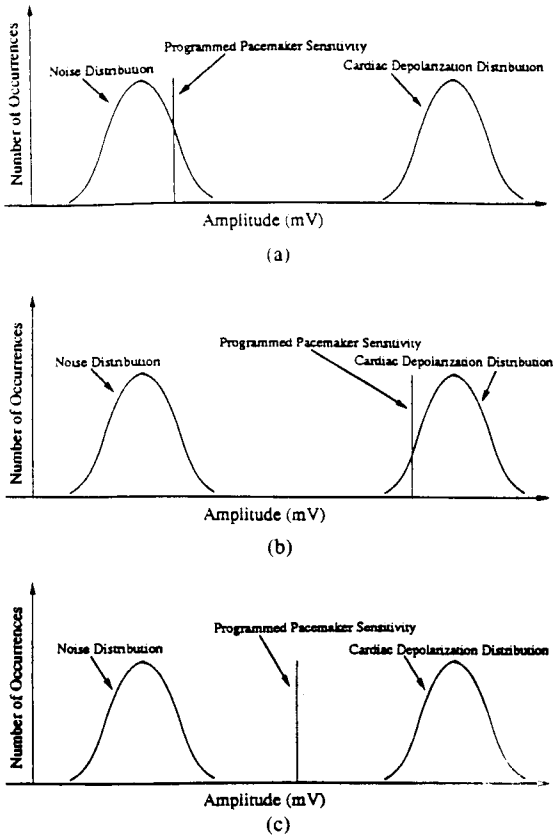

Fig. 8. Relationship among pacemaker sensitivity, spontaneous cardiac depolarizations, and noise. Cardiac depolarization and noise amplitude are represented by Gaussian distributions. (a) Programmed pacemaker sensitivity is set such that oversensing occurs. (b) Pacemaker sensitivity is set such that undersensing occurs. (c) Correct placement of sensing threshold.

decreasing manner. Concurrently, linear decreases in cycle length cause an exponential increase in AV conduction time [10]. In order to simulate Wenckebach periodicity and high degree block, a simple constant delay or linear AV response will not suffice; therefore, a formulation accounting for higher order AV function was used in our model. This is based on the work of Heethaar *et al.* [10], [11] who quantified the effect of changes in cycle length on AV nodal conduction time in rats, and later confirmed by Teague *et al.* [12] in humans.

1) Computer Implementation of AV Nodal Conduction Time: Because the works of Heethaar and Teague remain the classic quantitative description of the AV nodal input/output relationship, the Hagen methodology [13] of combining their results was implemented in the model described here. The Heethaar formulation [10] of the influence of previous cycle lengths on the current AV nodal conduction time is described as

$$g_n = \rho(\tau_n) + \sum_{j=1}^{4} \rho(\tau_{n-j}) e^{-\lambda \Sigma_{i=0}^{j-1} \tau_n - 1} \tag{6}$$

where

$$\rho(\tau_n) = g_{n,\infty}(1 - e^{-\lambda \tau_n}) \tag{7}$$

and where g_n is the AV conduction time following the nth cycle length, τ_n is the PP interval (cycle length) preceding g_n. $g_{n,\infty}$ is the AV conduction interval at steady state (as time $\rightarrow \infty$) with cycle length τ_n, τ_{n-i} is the ith previous cycle length, and λ is the reciprocal of the time constant. In order to model AV block, Heethaar later showed [11] that $\rho(\tau_n)$ may be estimated by

$$\rho(\tau_n) = A_o e^{-\lambda \tau_n} + C \tag{8}$$

where A_o, C, and λ were heart-dependent constants and τ_n was the nth cycle length.

Teague, using the single atrial extra stimulus technique, showed the application of (6) to humans for the influence of one previous cycle length to be

$$z = Ae^{-B}x + C \tag{9}$$

where $z = A_2H_2$, $x = A_1A_2$, $C = A_1H_1$, and A and B were patient-dependent constants.

Hagen combined (6) and (9) to form

$$g_n = \alpha \sum_{i=1}^{6} a_i e^{(-CL_{n-i}/\beta)} + \gamma. \tag{10}$$

In (10), g_n is the AV conduction time for cycle n in milliseconds corresponding to (6). The α term is a patient-specific constant which quantifies the magnitude of AV nodal response and, when multiplied by a_1, corresponds to A in (9). The coefficients a_1– a_6 are a series of exponentially decreasing constants representing the fractional contribution of the previous cycle length to the current AV conduction time. Each weighting coefficient corresponds to an $e^{-\lambda \Sigma \tau_{n-i}}$ term in (6). The cycle length CL_{n-i} refers to the ith previous PP interval and is identical to τ in (6). The term β corresponds to $1/\lambda$ in (6) and to $1/B$ in (9), and represents the rate of increase in the AV conduction time g_n as prior cycle lengths are shortened. The term γ is the steady-state AV conduction time as the cycle length approaches ∞. Values used for these patient-specific parameters are calculated off line directly from AV nodal conduction curves using a convergent iterative solution for nonlinear formulas described by Pennington [14].

Simulation of AV nodal conduction occurs as follows. After atrial or ventricular depolarization and determination of non accessory pathway conduction, g_n from (10) (which is equivalent to t_{CT}) is calculated. If $g_n \leq t_{CT_{\text{LIM}}}$, conduction is permitted through the node with conduction time of each AV node vertex equal to $g_n/2$. If, however, $g_n > t_{CT_{\text{LIM}}}$, then conduction is blocked at the AV node as the node is (effective) refractory. The parameter $t_{CT_{\text{LIM}}}$ is the AV conduction time corresponding to the effective refractory period.

E. Cardiac Rhythms Simulated

Normal conduction system parameter values, such as electrophysiologic refractory periods, which could be applied to the model for rhythm specification were derived from a classic text [15]. Table II shows a parameter specification file for a typical simulation of normal sinus rhythm. For the simulation of arrhythmias, these values were altered in an electrophysiologic manner. For example, in sinus bradycardia, the sinus and atrial vertex automatic (escape) interval times would be increased. For intermittent sino–atrial block, the atrial conduction probability would be decreased to a number

TABLE II
RHYTHM SPECIFICATION FILE EXAMPLE—NORMAL SINUS RHYTHM

		Automatic Interval		Antero Interval		Retro Interval		Accessory Interval		Phase		Probabilities			
Vertex	ERP	L	H	L	H	L	H	L	H	Shift	Ect	Ante	Ret	Auto	Acc
S	325	850	860	X	X	5	10	X	X	0	0	X	0	1	X
A	260	900	920	0	5	20	25	70	80	0	0	1	0	1	0
N_P	400	1000	1050	5	10	X	X	X	X	0	X	1	0	1	X
N_D	400	1000	1050	X	X	30	35	X	X	0	0	1	0	1	X
V	240	1500	2000	15	20	X	X	70	80	0	0	1	X	1	0
P_A	0	0	0	0	0	X	X	X	X	0	X	X	X	0	X
P_V	0	0	0	0	0	X	X	X	X	0	X	X	X	0	X

From top, the SA nodal (S), atrial (A), proximal AV nodal (N_P), distal AV nodal (N_D), ventricular (V), parasystolic atrial (P_A), and parasystolic ventricular (P_V) vertices are represented. Abbreviations: Accessory (or acc) = accessory pathway, Antero (or ante) = anterograde pathway, Auto = Automatic (escape), Ect = ectopic, ERP = effective refractory period, H = high value, L = low value, Phase Shift = offset for vertex timing, Probabilities = probability of the type of conduction given below, Retro (or ret) = retrograde pathway, X = not used (don't care). Anterograde, retrograde, and accessory intervals refer to conduction times. Parasystolic vertices are disabled unless nonzero values are entered.

TABLE III
CARDIAC RHYTHMS SIMULATED

Normal sinus rhythm
Sinus Arrhythmia
Sinus tachycardia, Sinus bradycardia, Sinus arrhythmia, SA node block
Atrial Arrhythmia
Premature atrial depolarizations, Atrial parasystole, Atrial bigeminy, Atrial trigeminy
Supraventricular tachycardia, Atrial flutter
Junctional Arrhythmia
Premature junctional depolarizations, AV nodal rhythm, AV nodal tachycardia, first degree AV block, second degree (Mobitz I and II) AV block third degree AV block.
Ventricular Arrhythmia
Premature ventricular depolarizations, Ventricular parasystole, Ventricular bigeminy, Ventricular trigeminy, Ventricular tachycardia, Ventricular flutter

less than 1. For random premature ventricular depolarizations, the ventricular ectopic probability would be increased to a number greater than 0. Atrial and ventricular bigeminies and trigeminies involve specifying the parasystolic vertices and including an appropriate phase shift. Supraventricular tachycardias with block can be simulated by increasing the AV nodal refractory period and/or decreasing the atrial escape rate. The dynamic characteristics of the AV node are changed by adding another line to the specification file which specifies α, β, γ, and $t_{CT_{\mathrm{LIM}}}$ for anterograde and retrograde conduction. This is necessary for simulating Wenckebach AV block.

A concise listing of possible simulated cardiac rhythms is shown in Table III. Model output consists of continuously generated ladder diagrams which are a tool the electrophysiologist uses to denote the sequence of cardiac activation. Ladder diagrams generated by the model designate exact timing of atrial, AV nodal, and ventricular activation. The output also indicates classified atrial and ventricular morphology, pacemaker function, and noise (Figs. 10–14). A simulated ECG output (Fig. 15) with three ventricular morphologies (normal, abnormal, and paced) and two atrial morphologies (normal and abnormal/paced) is available as well.

F. Implementation of Pacemaker Timing Algorithms

Atrial and ventricular pacing/sensing electrodes are conceptually attached to A and V vertices, which are then connected through leads to a pulse generator of specified mode and parameters. The pacemaker model controls *ap* and *vp* output in Fig. 1. Algorithms for 12 antibradycardia pacing modes

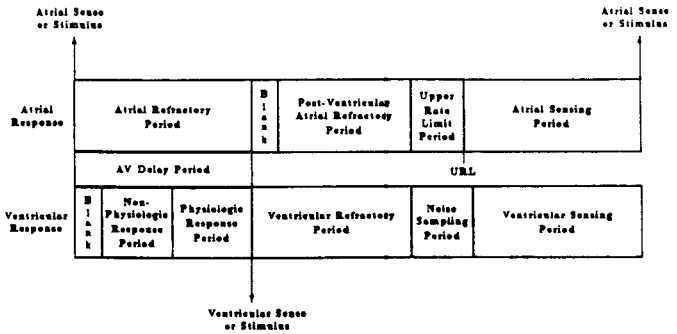

Fig. 9. Timing cycle for a typical, generic DDD pacemaker used in the simulation of Figs. 11–15 modified from Garson *et al.* [21]. See text for a description of pacemaker intervals. Table IV gives the pacemaker parameter values used in these simulations. URL = upper rate limit.

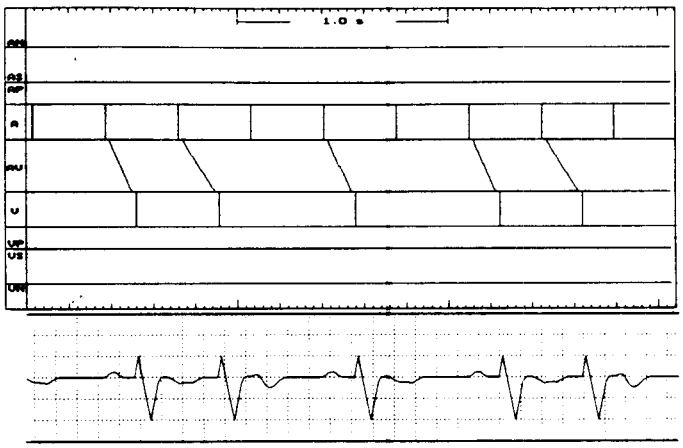

Fig. 10. Ladder diagram output of the heart model simulation of 3 : 2 alternating with 2 : 1 Wenckebach block. The solid vertical lines in the A channel represent normal atrial depolarizations; the diagonal lines through the AV channel represent conduction through the AV node; and the solid vertical lines in the V channel represent normal ventricular depolarization. The remaining channels (not used here) refer to pacemaker activity. The corresponding simulated ECG tracing output of the model has been pasted at the bottom of the figure.

are included in the pacemaker model. These are AOO, VOO, DOO, AAI, AAT, VVI, VVT, VAT, DVI (committed and noncommitted), VDD, DDI, and DDD modes as identified by the first three letters of the NASPE/BPEG code [16]. Briefly, the first letter of the code refers to the chamber(s) paced, the second letter to the chamber(s) sensed, and the third letter to the response of the pacemaker to sensed depolarizations.

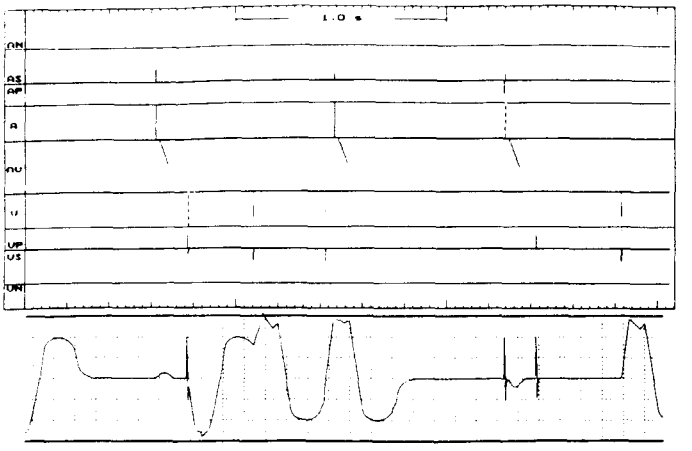

Fig. 11. Ladder diagram output of the simulation of ventricular failure-to-capture in a DDD pacemaker during third degree AV block with occasional premature ventricular depolarizations. The mean cardiac stimulation threshold was tripled, causing intermittent failure-to-capture. Vertical lines in the AP and VP channels represent atrial and ventricular pacing stimuli, respectively. A corresponding paced depolarization is indicated by a dashed line in A or V. Ectopic depolarizations are indicated by dotted lines in A and V channels. Blocked AV nodal conduction is designated by the shortened diagonal line in the AV channel. Long, solid vertical lines in the AS and VS channels represent atrial and ventricular sensed depolarizations, while short, solid lines represent pacemaker refractory period sensing. The second ventricular pacemaker stimulus fails to capture. This results in an escape ventricular depolarization which follows. The second and third ventricular depolarizations are also ectopic. The third ventricular depolarization causes the subsequent atrial depolarization to occur during the postventricular atrial refractory period of the pacemaker. The simulated ECG output is given below.

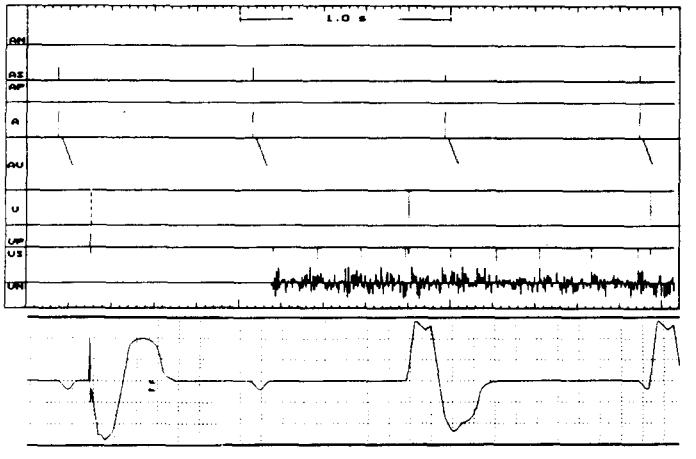

Fig. 12. Ladder diagram output of the simulation of ventricular oversensing in a DDD pacemaker during third degree AV block. The probability of atrial and ventricular noise episodes has been increased to occur approximately every 10 s. Also, noise standard deviations have been increased. Instantaneous atrial and ventricular noise are indicated on the AN and VN channels, respectively. Long, dotted lines in VS indicate noise sensing, which occurs in the ventricular channel at the end of each ventricular refractory period, causing inhibition of ventricular pacing. The ventricle depolarizes at the escape rate. See Figs. 10 and 11 for a description of the remaining symbols.

(A = atrium, V = ventricle, D = atrium and ventricle, 0 = none, I = inhibited, T = triggered, and D = inhibited and triggered.) Sensing pacemakers will inhibit pacemaker output (ap and vp in Fig. 1) in the appropriate chamber when a sensed depolarization occurs outside of pacemaker programmed refractory and blanking periods.

Since DDD pacemaker algorithms are the most complex and vary most between manufactures, HPI simulations of this mode

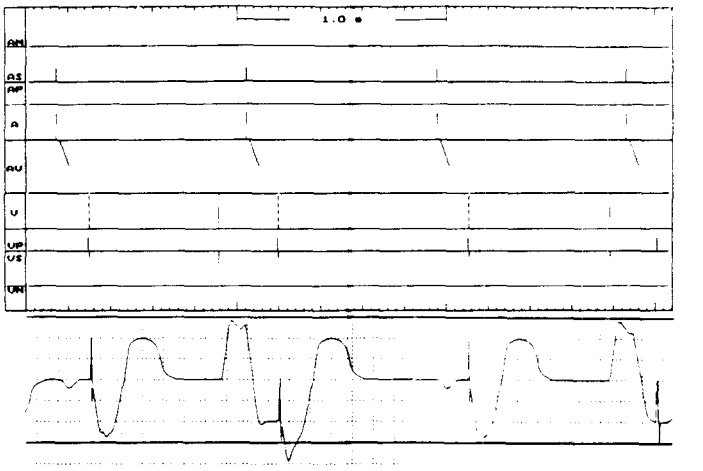

Fig. 13. Simulation of atrial to ventricular crosstalk in a DDD pacemaker. The first atrial stimulus causes noise which is sensed by the ventricular lead. This causes early pacing (termed *safety pacing*) by the ventricular lead in this pacemaker. The second atrial stimulus does not produce noise, and therefore the ventricular stimulus occurs after the normal AV interval. See Figs. 10 and 11 for a description of the symbols used.

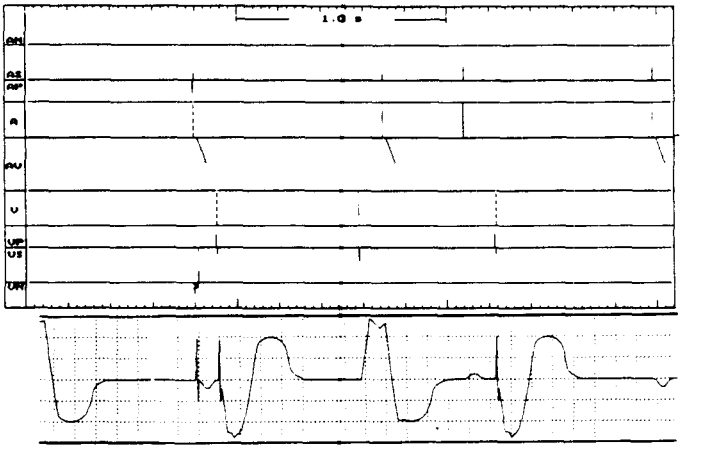

Fig. 14. Simulation of ventricular undersensing in a DDD pacemaker. Because of a decrease in the spontaneous depolarization mean amplitude, the second and fifth ventricular depolarizations (which are ectopic) are not sensed. Nonsensing caused by inadequate sensitivity is represented by the long, dashed line in the VS channel. This results in sensing of the following atrial stimulus which otherwise would have been unsensed because of the postventricular atrial refractory period of the pacemaker. Sensing of the atrial depolarization causes ventricular pacing after the pacemaker programmed AV interval. The first instance results in ventricular capture because the pacing stimulus occurs when the ventricular vertex is excitable. In the second instance, the ventricular pacing stimulus does not capture the ventricle because the vertex is refractory. See Figs. 10 and 11 for a description of the remaining symbols.

were emphasized. The pacing model includes sophisticated pacemaker algorithms by incorporating special-purpose blanking/refractory intervals which may be overridden, if necessary, in modeling a specific pacemaker.

The DDD timing cycle used in the results presented (Figs. 10–15) is shown in Fig. 9 and the values for each interval are given in Table IV. A generic DDD algorithm is used which has features common to many pacemakers. The cycle-to-cycle timing sequence depends on the escape interval from a ventricular sense or stimulus to the subsequent atrial stimulus (ventricular-based timing). Fig. 9 shows that following an atrial sense or stimulus is the *AV delay period*. During

this period, the atrial channel of the pacemaker is refractory to further sensing. In the ventricular channel, a blanking period occurs following an atrial stimulus which is designed to prevent false inhibition or early (*safety*) pacing of the ventricular output. Following the *ventricular blanking period* is the *nonphysiologic response period*. If a sense occurs during this interval, early (*safety*) pacing results at the end of the interval. This is to prevent pacing inhibition because of sensed noise and pacing at the end of the *AV delay period* which could cause capture during the vulnerable period of ventricular repolarization. Next is the *physiologic response period* during which time ventricular sensing is expected if AV conduction is intact. A ventricular sense during this interval causes inhibition of ventricular pacing; otherwise, pacing occurs at the end of the *AV delay period*. Following a ventricular sense or stimulus, an *atrial blanking period* and *postventricular atrial refractory period* (PVARP) occur in the atrial channel. This is usually collectively referred to as the PVARP. During PVARP, atrial senses are ignored. The PVARP aids in preventing pacemaker-mediated tachycardias which may result in DDD pacemakers from retrograde conduction or atrial tachyarrhythmias. Following PVARP is the *upper rate limit period*. Pacemakers have different techniques for limiting the upper rate behavior and allowing a smooth transition to the upper rate limit. The method chosen here increases the AV interval by the amount of the *upper rate limit period* remaining after an early atrial depolarization. Following the *upper rate limit period* is an interval of normal atrial sensing. After a ventricular event, the ventricular channel becomes refractory to ventricular depolarizations during the *ventricular refractory period*. Following this period, a *noise sampling period* occurs during which time any sensing is assumed to be noise and the pacemaker enters a noise reversion mode of asynchronous pacing. After the *noise sampling period*, the pacemaker enters a ventricular sensing interval. If a ventricular sense precedes an atrial event, the timing sequence begins as shown in Fig. 9 at the ventricular sense.

In addition to implementation of pacemaker timing algorithms as described above, pacemaker simulation determines whether: 1) pacing stimuli have sufficient energy to depolarize myocardium, 2) spontaneous depolarizations have sufficient amplitude to be sensed, and 3) noise was sensed. This information is reported to the ladder diagram in terms of coded markers and to a text file as sentence explanations.

G. Pacemaker Capture of Myocardium

Failure-to-capture is a result of the cardiac stimulation threshold exceeding the pacemaker's depolarizing energy.[3] In practice, at implant, the clinician determines the patient's cardiac stimulation threshold level, and sets the pacemaker voltage or current output and pulse width accordingly. Since stimulation threshold may typically increase to five times the necessary charge at implant during the first several weeks postimplant, the clinician includes a safety factor in the programmed pacemaker output. This safety factor may later be decreased as electrode encapsulation occurs, usually causing the stimulation threshold to plateau at a level approximately two times its initial value. Because of the changing threshold and desire to maximize battery life, failure-to-capture may occur. In order to simulate this occurrence, parameters to describe the cardiac stimulation threshold and pacemaker output are included in the described model of heart–pacemaker interaction.

In the model, cardiac stimulation threshold is assumed to be normally distributed. The stimulation threshold is specified as an energy (in μJ), whose mean and standard deviation are variables defined in an input file. The atrial and ventricular thresholds are defined separately.

Each time the pacemaker stimulates atrial or ventricular myocardium, a pseudorandom number with Gaussian distribution T_G representing the cardiac stimulation threshold is generated using the *Box–Muller* transformation of a uniform random variable [18]. T_G is compared to the output energy of the pacemaker (also in μJ). This output energy, E_{PO}, is calculated using programmed pacemaker parameters and lead-myocardial output impedence as

$$E_{PO}(\mu\text{J}) = \frac{V^2}{Z} \times PW \tag{11}$$

where V is the pacemaker pulse amplitude in V, Z is the lead-myocardial output impedence in kΩ, and PW is the pulse width in ms.[4] V and PW are programmable pacemaker parameters, and may be changed in the HPI simulation. The value of Z is set at the standard of 0.510 kΩ [19], although it may also be changed.

Fig. 7 shows the graphical relationship between the stimulation threshold and the pacemaker output energy in two cases. In Fig. 7(a), the output energy is above the threshold with near 100% certainty, while in Fig. 7(b), the pacemaker is expected to fail to capture approximately 40% of the time because of an incorrectly low setting of pacemaker output.

H. Pacemaker Sensing of Myocardium

Permanent pacemakers are designed to sense spontaneous cardiac electrical activity. Most pacing algorithms use bandpass-filtered electrogram amplitude to determine if a cardiac depolarization has occurred. Since electrogram amplitude threshold (sensitivity) is commonly the only parameter available to the clinician for programming, this was the only parameter included in the pacemaker model.

In addition to sensing same chamber myocardial depolarization, signals such as myocardial repolarization, cross-chamber depolarization, nonmyocardial myopotential, and electromagnetic interference[5] may be sensed (incorrectly) as well. These interfering signals may be sensed due to overlapping frequency spectra with desired events. A noise feature which mimics these events is included in the model.

[3] This effect could also result from attempted myocardial depolarization during the absolute or relative myocardial refractory periods, insufficient contact between the lead and the myocardium, or lead fracture.

[4] This equation assumes a constant voltage generator included in nearly all modern-day permanent pacemakers.

[5] These four types of interference are hereafter referred to as *noise*.

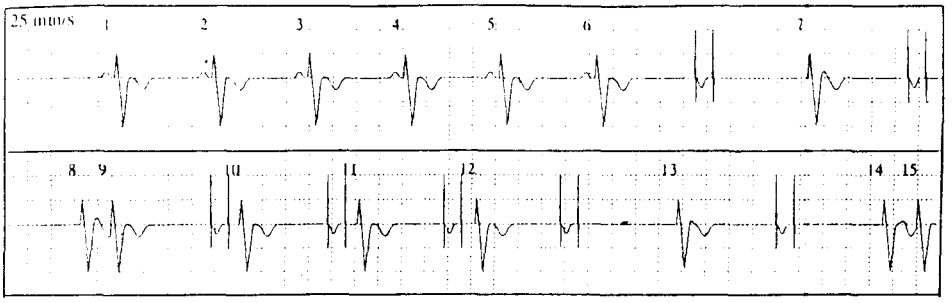

Fig. 15. ECG simulation of ventricular failure to capture with an underlying Wenckebach AV block. Beats 1–6 display normal conduction. The intrinsic atrial rate slows after 6, resulting in atrial pacing and capture. AV conduction also slows, resulting in ventricular pacing, but failure to capture. (The stimulation threshold exceeds the pacemaker output.) Beat 7 is an escape AV nodal depolarization with atrial retrograde activation. The following sequence through beat 8 is identical to the sequence prior to 7. Beat 9 is an early supraventricularly conducted ventricular depolarization. Beat 10 begins a Wenckebach sequence which concludes with the nonconducted P wave following beat 12. The phenomenon is visible because of consistent ventricular failure to capture. Beat 13 is again an AV nodal escape, and a familiar sequence concludes the passage. All ventricular depolarizations are of normal morphology. P waves with positive polarity are normal, and P waves with negative polarity are of paced morphology. 25 mm/s = 200 ms/division.

In the HPI model described, spontaneous cardiac depolarization amplitude and noise amplitude are each considered normally distributed. As in the case of cardiac stimulation threshold, means and standard deviations for depolarization and noise amplitude are specified in data input files. Sensitivity and noise are set individually for atrial and ventricular chambers. In addition to external noise sources which may affect one chamber or the other, *crosstalk* noise may be specified. This is equivalent to the interference that occurs in dual-chamber devices when a pacemaker stimulus intended to depolarize one chamber is sensed by the alternate chamber and causes inhibition or early stimulus triggering there.

The sensitivity threshold is a linear, one-dimensional decision boundary in the pattern recognition sense. The pacemaker model will sense signals with amplitude greater than the sensitivity threshold, and ignore signals at amplitudes less than this value. The model sensitivity is empirically set such as is done by the clinician at device implant. This is typically a value less than the spontaneous depolarization amplitude minus an adequate safety factor, and yet greater than the expected noise amplitude. In rare cases, the two distributions may overlap, most often with unipolar sensing, and therefore an absolute threshold may not be found. Fig. 8 shows graphically two cases of incorrect setting of pacemaker sensitivity and one case where sensitivity was set to an adequate value.

I. Pacemaker Stimulation Output

Paced morphology output, *ap* and *vp*, are designated by dashed lines in the atrial or ventricular channel on the ladder diagram output. These represent morphologically distinct waveforms from normal (solid line) and abnormal (dotted line) waveforms.

If atrial and/or ventricular noise is specified, the instantaneous atrial noise amplitude is continuously displayed on the AN (atrial noise) channel and ventricular noise on the VN (ventricular noise) channel. Pacemaker simulation also includes a marker channel which indicates the manner of pacing and sensing response of the pacemaker algorithm. The symbols have been modeled after a manual ECG marker system deviced by Bernstein and Parsonnet [20]. The Bernstein–Parsonnet marker system was altered for use in the model simulation due to the continuous nature of the output display. Whenever a pacemaker is specified, appropriate markers are displayed on AP (atrial pace), VP (ventricular pace), AS (atrial sense), or VS (ventricular sense) channels. In addition to graphical display, a text file output indicates pacemaker and conduction system information in the form of word explanations and indicates the exact timing of these events for algorithmic verification and troubleshooting.

The simulated paced ECG output intentionally displays only the information typically available on a standard surface ECG. A third ventricular morphology representing a paced depolarization and nonchamber-specific pacing artifacts are presented.

III. Results

Cardiac rhythms shown in Table III and pacing protocols described above have been simulated using the model presented. A cardiac electrophysiologist reviewed simulations from each category, with and without the effects of artificial pacemakers, to validate correct model function. In order to illustrate model utility and output, several examples are shown here. Fig. 10 shows a simulation ladder diagram output of 3 : 2 alternating with 2 : 1 Wenckebach block as generated by the model. Block occurs at the proximal AV node when the calculated AV nodal conduction time exceeds the maximum conduction time corresponding to the effective refractory period.

Figs. 11–14 show the automatically generated simulation of a DDD pacemaker during a rhythm of third degree AV block with occasional premature depolarizations. The DDD parameters used in Figs. 11–15 are shown in Table IV. In order to simulate malfunction, cardiac and noise parameters were varied over reasonable ranges, while all pacemaker specifications were held constant. In Fig. 11, mean cardiac stimulation threshold has been tripled from 2 to 6 μJ, resulting in intermittent failure to capture. Fig. 12 gives an example of pacemaker noise oversensing. Since this pacemaker has no *noise sampling period* defined, inhibition of pacemaker output occurs during the noise episode. If a *noise sampling period* had been defined, triggering of atrial and ventricular stimuli would have occurred at the pacemaker's lower rate limit.

TABLE IV
DDD PACEMAKER PARAMETERS FOR FIGS. 11–15

Parameter	Value
Lower rate limit	60 beats/min
Upper rate limit	175 beats/min
Ventricular blanking period	20 ms
Nonphysiologic portion of AV interval	90 ms
Physiologic portion of AV interval	40 ms
Ventricular refractory period	200 ms
Atrial blanking period	0 ms
Ventricular noise sampling period	0 ms
Postventricular atrial refractory period	235 ms
PVARP extension	50 ms

Crosstalk noise via the atrial stimulus occurs intermittently in Fig. 13. The specified pacemaker in designed to trigger early (*safety pace*) if ventricular sensing occurs during a specific period following the atrial stimulus. This harmlessly avoids pacemaker inhibition in response to this noise. Fig. 14 shows an example of ventricular undersensing due to a decrease in mean ventricular electrogram amplitude from 6.0 to 3.0 mV.

Fig. 15 is an example showing the optional simulated ECG presentation of the model. The intrinsic rate slows and the AV interval lengthens with resulting AV sequential pacing from a DDD pacemaker. A Wenckebach AV block is seen on beats 10–13 since the ventricular pacing output consistently fails to capture.

IV. DISCUSSION

A model of HPI which simulates pacemaker function and malfunction in a variety of complex antibradycardia pacemakers has been described. The model consists of a signal flow network whose state transitions are controlled by multidimensional CPF's. These CPF's are a unique aspect of the network model which allow concise and electrophysiologic specification of particular cardiac rhythms. The structure of the model is such that it is not arrhythmia dependent, unlike some other conduction models. Also, the conduction system simulation described contains a mathematical input/output model of AV nodal conduction, which is based upon experimental data. Given this methodology, the conduction model may simulate 23 classes of arrhythmias.

This model of HPI is unique in including specification of cardiac, pacemaker, and noise distribution parameters which permit random simulation of pacemaker failure. Oversensing of noise, undersensing of spontaneous cardiac depolarizations, and failure of the pacemaker stimulus to depolarize myocardium may be simulated in the context of complex arrhythmias and sophisticated pacemakers. The simulation should prove useful in the

- development of pacemaker algorithms,
- education of personnel in pacing modes, pacemaker programmable settings, and pacemaker failure,
- Simulation of pacemaker pseudomalfunction (i.e., perceived pacemaker malfunction caused by pacemaker algorithm or programming),
- Determination of appropriate pacemaker therapy, given cardiac rhythm specification, and
- Development of systems for computerized arrhythmia and paced ECG diagnosis.

Complex models of the cardiac conduction system have been developed. Saxberg *et al.* [4] developed an anatomically and physiologically detailed model for the study of the effects of fiber orientation and the time dependence of local propagation parameters. Restivo *et al.* [5] have developed a detailed logical state model for simulation of ventricular reentrant arrhythmias. The purpose of the model presented here, however, was to simulate cardiac rhythm with the effect of artificial pacemakers in an efficient and simple manner.

Physiologic network models to study cardiac rhythm have been reported by Dassen *et al.* [17] and Hagen *et al* . [13]. These models are more complex in the specification of electrophysiologic conditions than the one described in this paper because of numerous pathway elements between junction points for which separate conduction velocities and refractory periods must be defined. The Chin model [8], based upon Petri net theory, requires separate structure and parameters for the modeling of each arrhythmia. In the Malik ten-element heart model [6], it is unclear how classes of arrhythmias are generated, and it appears not to be done in a clearly definable electrophysiologic manner. Also, the number of vertices changes in Malik's model, depending upon the rhythm simulated. In our model, the conduction system network is basic and remains identical for all arrhythmias. Refractory periods, conduction intervals, and probabilities of conduction are specified in a logical electrophysiologic manner at each vertex in order to simulate specific rhythms. In addition, none of the above models except Hagen's [13] includes a physiologic model of AV nodal conduction.

Earlier computer simulations of the interaction between cardiac rhythm and artificial pacing have also been designed [6], [21]–[26]. The rhythm and pacemaker models are of variable complexity. Malik *et al* . have used their most detailed heart model [23] (6390 hexagonal elements) to their simplest [6] (ten elements) for HPI simulation. Malik *et al.* [27] also described a pacemaker timing model represented by traditional state diagrams which mimics the usual algorithmic design and implementation procedure. Byrd and Byrd [22] used a deterministic physiologic simulator, but included an extensive pacemaker library of 125 pacemaker models. Dassen *et al.* [24] simulated the action of DDD and antitachycardia pacemakers using the model from [17], and Åhlfeldt *et al.* [26] demonstrated DDD pacing using a detailed network of 115 cardiac elements for which "action potentials" were specified.

None of these HPI simulations previously reported has modeled pacemaker malfunction resulting from pacemaker output and sensitivity considerations. In the model described here, simulation of pacing and sensing failure is performed through the use of appropriate cardiac, pacemaker, and noise distribution parameters.

Although the pacemaker model includes many of the most sophisticated pacing modes and algorithms, certain modes and algorithms are not included. For example, *rate-responsive* pacemakers which sense metabolic indicators, responding by a change in pacing rate, are not simulated here. Also, manufacturer-specific algorithms such as *rate smoothing* [28], which eliminate large cycle-to-cycle variations in rate by preventing the paced interval from changing by more than a programmed percentage from one cardiac cycle to the next, are not simulated. Inclusion of such modes and algorithms is proposed as future work.

The HPI model described was specifically developed and was used in the design and testing of a knowledge-based, automated, paced ECG analysis system for explication of pacemaker malfunction [1], [2]. The model facilitated development of this system by providing insight into algorithmic development and by providing a training and test set which reduced the degree of clinical testing required.

ACKNOWLEDGMENT

The authors thank Dr. L. DiCarlo for his careful review of simulation results to verify correct model function.

REFERENCES

[1] S. E. Greenhut, "Computer modelling and interpretation of paced electrocardiograms for analysis of pacemaker function," Ph.D. dissertation, Univ. Michigan, Bioengineering Program, 1991.
[2] S. E. Greenhut, J. M. Jenkins, and L. A. DiCarlo, "Automated analysis of DDD pacemaker electrocardiograms for interpretation of pacemaker function and failure," *PACE*, vol. 14, p. 671, 1991 (abstract).
[3] M. Malik, T. Cochrane, and A. J. Camm, "Computer simulation of the cardiac conduction system," *Comput. Biomed. Res.*, vol. 16, pp. 454–468, 1983.
[4] B. E. H. Saxberg, M. P. Grumbach, and R. J. Cohn, "A time dependent anatomically detailed model of cardiac conduction," in *Proc. Comput. Cardiol.*, pp. 401–404, 1985.
[5] M. Restivo, W. Craelius, W. B. Gough, and N. El-Sherif, "A logical state model of reentrant ventricular activation," *IEEE Trans. Biomed. Eng.*, vol. 37, pp. 344–353, 1991.
[6] M. Malik, T. Cochrane, and A. J. Camm, "Computer simulation of cardiac rhythm and artificial pacemakers using a ten-element heart model," *Comput. Biomed. Res.*, vol. 19, pp. 237–253, 1986.
[7] L. S. Bobrow and M. A. Arbib, *Discrete Mathematics: Applied Algebra for Computer and Information Science*. Philadelphia, PA: Saunders, 1974, pp. 68–162, 498–513.
[8] T. M. Chin and A. S. Willsky, "Stochastic Petri net modeling of wave sequences in cardiac arrhythmias," *Comput. Biomed. Res.*, vol. 22, pp. 136–159, 1989.
[9] M. K. Molloy, "Performance analysis using stochastic Petri nets," *IEEE Trans. Comput.*, vol. C-31, pp. 913–917, 1982.
[10] R. M. Heethaar, J. J. D. van der Gon, and F. L. Meijler, "Mathematical model of A-V conduction in the rat heart," *Cardiovas. Res.*, vol. 7, pp. 105–114, 1973.
[11] R. M. Heethaar, R. M. de vos Burchart, J. J. D. van der Gon, and F. L. Meijler, "A mathematical model of A-V conduction in the rat heart. II. Quantification of concealed conduction," *Cardiovas. Res.*, vol. 7, pp. 542–556, 1973.
[12] S. Teague, S. Collins, D. Wu, P. Denes, K. Rosen, and R. Arzbaecher, "A quantitative description of normal AV nodal conduction curve in man," *J. Appl. Physiol.*, vol. 40, pp. 74–78, 1976.
[13] G. T. Hagen, W. R. M. Dassen, T. E. Bump, and R. C. Arzbaecher, "Arrhythmia simulation and explication by computer modelling of cardiac conduction," in *Proc. Comput. Cardiol.* pp. 217–220, 1983.
[14] R. H. Pennington, *Introductory Computer Methods and Numerical Analysis*. Toronto, Canada: Macmillan, 1970, pp. 421–427.
[15] M. E. Josephson and S. F. Seides, *Clinical Cardiac Electrophysiology: Techniques and Interpretations*. Philadelphia, PA: Lea & Febiger, 1979, p. 44.
[16] A. D. Bernstein, A. J. Camm, R. D. Fletcher, R. D. Gold, A. F. Rickards, N. P. D. Smyth, S. R. Spielman, and R. Sutton, "The NASPE/BPEG pacemaker code for antibradyarrhythmia and adaptive-rate pacing and antitachyarrhythmia devices," *PACE*, vol. 10, pp. 794–799, 1987.
[17] W. Dassen, P. Brugada, D. Richards, M. Green, B. Heddle, and H. Wellens, "A mathematical model of the conduction system to study the mechanisms of cardiac arrhythmias," in *Proc. Comput. Cardiol.* 1982, pp. 193–196.
[18] W. H. Press, B. P. Flannery, S. A. Teukolsky, and W. T. Vetterling, *Numerical Recipes in C: The Art of Scientific Computing*. New York: Cambridge Univ. Press, 1988, pp. 214–217.
[19] S. Furman, D. L. Hayes, and D. R. Holmes, *A Practice of Cardiac Pacing*, 2nd ed. Mount Kisco, NY: Futura, 1989, p. 60.
[20] A. D. Bernstein and V. Parsonnet, "Notation system and overlay diagrams for the analysis of paced electrocardiograms," *PACE*, vol. 6, pp. 73–80, 1983.
[21] A. Garson, T. Coyner, C. E. Shannon, and P. C. Gillette, *Practical Cardiac Pacing*. Baltimore, MD: Williams & Wilkins, 1986, pp. 181–270.
[22] C. B. Byrd and C. L. Byrd, "A computerized system for modeling pacemaker rhythms," *J. Electrocardiol.*, suppl. to vol. 20, pp. 28–33, 1987.
[23] M. Malik, A. Nathan, and A. J. Camm, "Computer simulation of dual chamber pacemaker algorithms using a realistic heart model," *PACE*, vol. 8, pp. 579–588, 1985.
[24] W. R. M. Dassen, K. den Dulk, A. P. M. Gorgels, P. Brugada, and H. J. J. Wellens, "Evaluation of pacemaker performance using computer simulation," *PACE*, vol. 8, pp. 795–805, 1985.
[25] M. Malik and A. J. Camm, "Computer modeling of cardiac rhythm disturbances and heart–pacemaker interaction," *PACE* , vol. 11, pp. 2101–2109, 1988.
[26] H. Åhlfeldt, H. Tanaka, M. E. Nygards, T. Furukawa, and O. Wigertz, "Computer simulation of cardiac pacing," *PACE*, vol. 11, pp. 174–184, 1988.
[27] M. Malik, T. Cochrane, D. W. Davies, and A. J. Camm, "Clinically relevant computer model of cardiac rhythm and pacemaker/heart interaction," *Med. Biol. Eng. Comput.*, vol. 25, pp. 504–512, 1987.
[28] Cardiac Pacemakers Inc., *DELTA Model 925 Physician's Manual*. St. Paul, MN: Cardiac Pacemakers Inc., 1989, pp. 19–33.

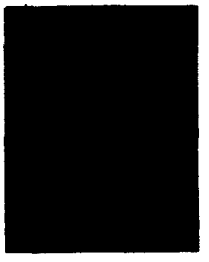

Saul E. Greenhut (S'89–M'91) received the B.S.E. degree in engineering science and the M.S. and Ph.D. degrees in bioengineering from the University of Michigan, Ann Arbor, in 1983, 1984, and 1991, respectively.

In the interim, he served as Research Engineer in the Pacemaker Clinic at the Newark Beth-Israel Medical Center, Newark, NJ, and as Computer Coordinator in Cardiology at William Beaumont Hospital, Royal Oak, MI. During his doctoral studies, he was a Research Assistant in the Departments of Cardiology and Electrical Engineering, as part of the Medical Computing Laboratory, at the University of Michigan. He is currently a Research Scientist in the Applied Research Division of Telectronics Pacing Systems, Englewood, CO. His research interests include signal processing, pattern recognition, and electrophysiology with specific applications to implantable pacemakers and defibrillators.

Janice M. Jenkins (S'75–M'78–SM'84) received the B.S. degree in mathematics and computer science and the M.S. and Ph.D. degrees in computer engineering from the University of Illinois at Chicago in 1974, 1976, and 1978, respectively.

She was a member of the faculty of Northwestern University, Evanston, IL, from 1979 to 1980, with an appointment in Internal Medicine and in Electrical Engineering and Computer Science. She is currently a Professor of Electrical Engineering and Computer Science at the University of Michigan, Ann Arbor, a member of the Bioengineering Faculty, and Director of the Medical Computing Laboratory and the Digital Design Laboratory. Her research interests are digital signal processing of the electrocardiogram, and implantable devices for treatment of cardiac arrhythmias.

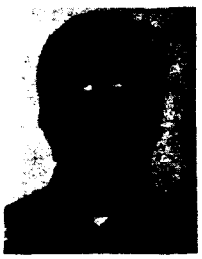

Robert S. MacDonald received the B.S.E. degree in computer engineering and the B.S.E. degree in electrical engineering in 1985, and the M.S.E. degree in computer engineering in 1987, all from the University of Michigan, Ann Arbor.

He is a Research Engineer at the Applied Research Laboratories of the University of Texas. His research interests include machine perception, signal processing, and real-time computing.

Mr. MacDonald is a member of the IEEE Computer Society and the IEEE Signal Processing Society.